Angle-resolved photoemission study of Ni-intercalated $1T$-TiS_2

T. Matsushita,* S. Suga,† and A. Kimura‡
Department of Material Physics, Faculty of Engineering Science, Osaka University, Machikaneyama, Toyonaka, Osaka 560-8531, Japan

H. Negishi and M. Inoue
Department of Materials Sciences, Faculty of Science, Hiroshima University, Higashi Hiroshima 739-8526, Japan
(Received 11 January 1999)

Angle-resolved photoemission spectra have been measured to study the electronic structures of Ni intercalated layered compound $Ni_{1/3}TiS_2$. The results have shown that some new bands appear in $Ni_{1/3}TiS_2$ and the dispersions of most other bands are strongly modified compared with TiS_2. It is clarified that the new band near the Fermi level (E_F) is the split-off state or the bonding state between the final states originating from the $|d^1(t_{2g})\rangle$ and $|d^2(t_{2g},e_g)\underline{L}\rangle$ initial states, where $\underline{L}$ stands for the S $3p$ hole state. Another new band observed at $\sim$1 eV below E_F is hardly dispersive and attributed to the Ni $3d_{z^2}$-Ti $3d_{z^2}$ bonding state. The Ni $3d$''e_g''-S $3p$ bonding states are observed in the larger binding energy region. Knowledge of hybridizations among the $3d$ states of the intercalant, Ti $3d$ states, and S $3p$ states are essential to interpret the physical properties of $Ni_{1/3}TiS_2$. [S0163-1829(99)02727-7]

I. INTRODUCTION

A large number of studies have been carried out to know the electronic structures of the host $1T$-TiS_2 by means of angle-resolved photoemission,[1,2] inverse photoemission,[3] and band calculations.[4] $1T$-TiS_2 has the CdI_2-type layer structure, which consists of a Ti layer sandwiched in two sulfur layers. Six sulfur atoms surround the Ti atom with nearly octahedral coordination. The outer sulfur layers are weakly coupled with the adjacent sulfur layers by the van der Waals force.

The $3d$ transition metal (TM) intercalated $1T$-TiS_2, M_xTiS_2 (M=Mn, Fe, Co, and Ni), shows various unusual physical properties compared with $1T$-TiS_2. Such properties depend dramatically on the guest atom species and its concentration.[5,6] Recent detailed studies have revealed itinerant behaviors of the intercalant M $3d$ electrons.[7,8] $Ni_{1/3}TiS_2$ has such a characteristic feature as the hole pockets as suggested from Hall measurements, in contrast to other intercalation compounds (M=Mn and Co) which have electronlike carriers. In the Ni intercalation compound, $Ni_{1/3}TiS_2$, the intercalant Ni atoms occupy the nearly octahedral interstitial sites in the van der Waals gap between the neighboring sulfur layers. The intercalant Ni atoms are known to form a $\sqrt{3}a\times\sqrt{3}a$ triangular-superlattice structure. In accord with the difference in the phase of such triangular superlattices, they are named *A*, *B*, and *C*. Representing the TiS_2 layer as *T*, the stacking of the whole layers is described as *TATBTCTATBTC* . . . along the *c* axis. The rhombohedral unit cell shown in Fig. 1 contains one Ni atom, three Ti atoms, and six S atoms. The band structure of $Ni_{1/3}TiS_2$ was recently calculated by the augmented-plane-wave (APW) method.[9,10] Their results have indicated that the hybridizations among the S $3p$, Ti $3d$, and Ni $3d$ states are important, and the rigid-band shift model is hardly applicable to this system. Ueda *et al.* performed ultraviolet-photoemission spectroscopy (UPS measurements) on M_xTiS_2 using synchrotron radiation in the photon energy range of $h\nu$ =32–120 eV. The symmetry and hybridization of the electronic states were discussed from the resonant behaviors.[11,12] Fujimori *et al.* performed x-ray-photoemission spectroscopy (XPS) of core levels and valence bands of M_xTiS_2.[13] Strong hybridizations among the M $3d$, Ti $3d$, and S $3p$ states are confirmed from these UPS and XPS results. Namatame *et al.* carried out angle-resolved inverse-photoemission-spectroscopy (ARIPES) on $Ni_{1/3}TiS_2$ and found the Ni $3d_{z^2}$-Ti $3d_{z^2}$ antibonding state.[14] Although the band den-

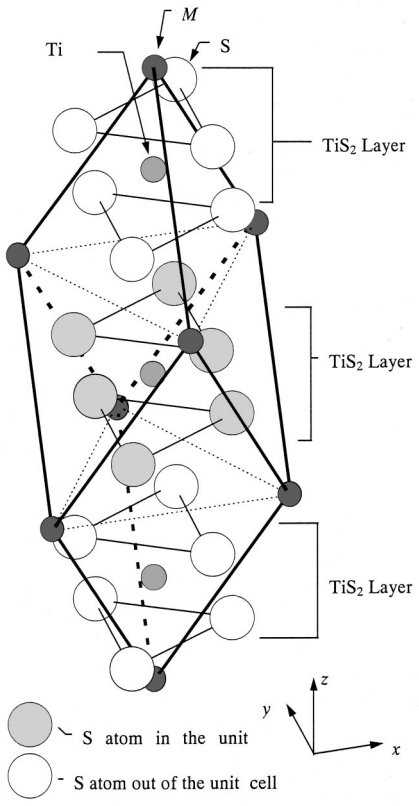

FIG. 1. The crystal structure of M_xTiS_2.

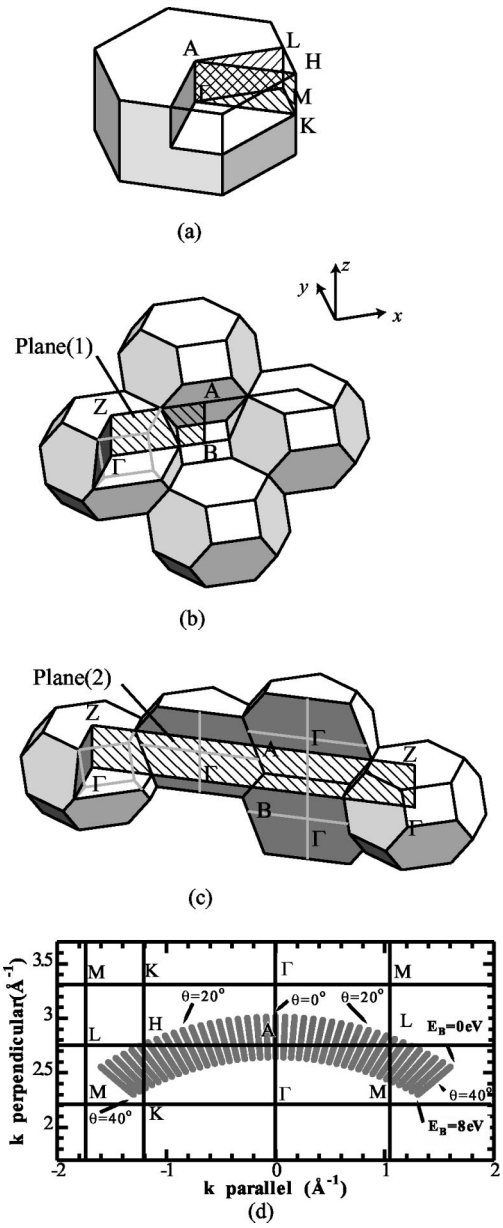

FIG. 2. The Brillouin zone of TiS_2 and $M_{1/3}TiS_2$. (a) BZ of $1T$-TiS_2. (b) and (c) BZ of $M_{1/3}TiS_2$. Plane (1) in (b) includes the axis equivalent to the $\Gamma(A)$-$M(L)$ direction of $1T$-TiS_2. Plane (2) in (c) includes the axis equivalent to the $\Gamma(A)$-$K(H)$-$M(L)$ direction. (d) The relation of k perpendicular and k parallel to the layer (surface) in our θ-dependent ARUPS experiment.

sity of states (DOS) was thus already studied for $Ni_{1/3}TiS_2$ by UPS and XPS, details of the band dispersions are not yet clarified due to the complexity of its band structures. In the present work, we report on the results of angle-resolved-ultraviolet-photoemission-spectroscopy (ARUPS) measurements on $Ni_{1/3}TiS_2$ in comparison with those of the mother crystal, $1T$-TiS_2. In the ARUPS measurement, knowledge of the details of the Brillouin zone (BZ) is required. The simple hexagonal BZ of mother crystal $1T$-TiS_2 is shown in Fig. 2(a). The BZ of $M_{1/3}TiS_2$ is shown in Figs. 2(b) and 2(c).

II. EXPERIMENT

The ARUPS measurement was performed with using synchrotron radiation in the photon energy range of 18–60 eV at the BL-18A beam line of the Photon Factory (PF), High Energy Accelerator Research Organization (KEK). This beam line is equipped with a constant deviation type grazing incidence monochromator and an electron energy analyzer of VG ADES 500 type with the angular resolution of about $\pm 1°$. The total energy resolution was set to about 300 meV in the present measurement. The light was incident onto the sample surface at 45° from the surface normal (p-polarized configuration). The electron energy analyzer was rotated in the horizontal plane including the $\Gamma(A)$-$M(L)$ or $\Gamma(A)$-$K(H)$ axis for the polar angle (θ) scanning while the photon energy ($h\nu$) was fixed at 28 eV. In addition, the normal photoemission spectra ($\theta = 0°$) were measured with changing $h\nu$. The measurements were performed at room temperature for both $1T$-TiS_2 and $Ni_{1/3}TiS_2$. The Fermi Energy E_F was determined by the UPS spectrum of an evaporated Au thin film.

The samples were cleaved in an ultrahigh vacuum preparation chamber with a pressure of low 10^{-10} Torr and immediately transferred onto a manipulator in an analyzer chamber with a base pressure of 5×10^{-11} Torr. The crystal orientation was determined by the low-energy electron diffraction (LEED) pattern which showed $\sqrt{3}\times\sqrt{3}$ super structure in $Ni_{1/3}TiS_2$. The sample was azimuthally rotated to make the $\Gamma(A)$-$M(L)$ or the $\Gamma(A)$-$K(H)$ orientation lie in the horizontal plane. The cleanliness of the surface was checked by O $1s$ XPS just before and after the ARUPS measurement.

III. RESULTS AND ANALYSIS

A. $1T$-TiS_2

Figure 3(a) summarizes the θ dependence of the ARUPS spectra of $1T$-TiS_2 measured at $h\nu = 28$ eV for the wave vector $k_\parallel$ (parallel to the surface) in the plane including the $\Gamma(A)$-$M(L)$ axis. The results taken along the $\Gamma(A)$-$K(H)$ axis are shown in Fig. 3(b). The normal ($\theta = 0°$) photoemission spectra are shown in Figs. 3(c). The spectra strongly depend on θ and $h\nu$. In particular, the spectra have shown a small peak just below E_F near the $M(L)$ point [$\theta \sim 26°$ in Fig. 3(a)], whereas the corresponding intensity is negligible for other θ.

In order to even resolve weak photoemission structures, we have deconvoluted the photoemission spectra. Conventional formulas for the angle-resolved photoemission spectroscopy are used to evaluate the momentum of the photoelectron. For the $\theta-(h\nu-)$ scanned spectra, the parallel (perpendicular) component of the photoelectron wave vector relative to the surface is calculated with using $k_\parallel = \sqrt{2mE_K/\hbar^2}\sin\theta$[$k_\perp = \sqrt{2m(E_K+V_0)/\hbar^2}$ where V_0 stands for the inner potential; the value of V_0 is determined as 11 eV by considering the symmetry of the experimentally derived band structure near the high symmetry point]. The values of k are calculated for all the observed structures. We plotted them on the k-E_B diagram along the $\Gamma(A)$-$M(L)$, $\Gamma(A)$-$K(H)$, and Γ-A axes as shown in Figs. 4(a), 4(b), and 4(c). In these figures, the bright (white) area corresponds to the observed bands.

When V_0 is determined, we can evaluate both $k_\parallel$ and $k_\perp$ components in the θ-dependent band mapping in the same

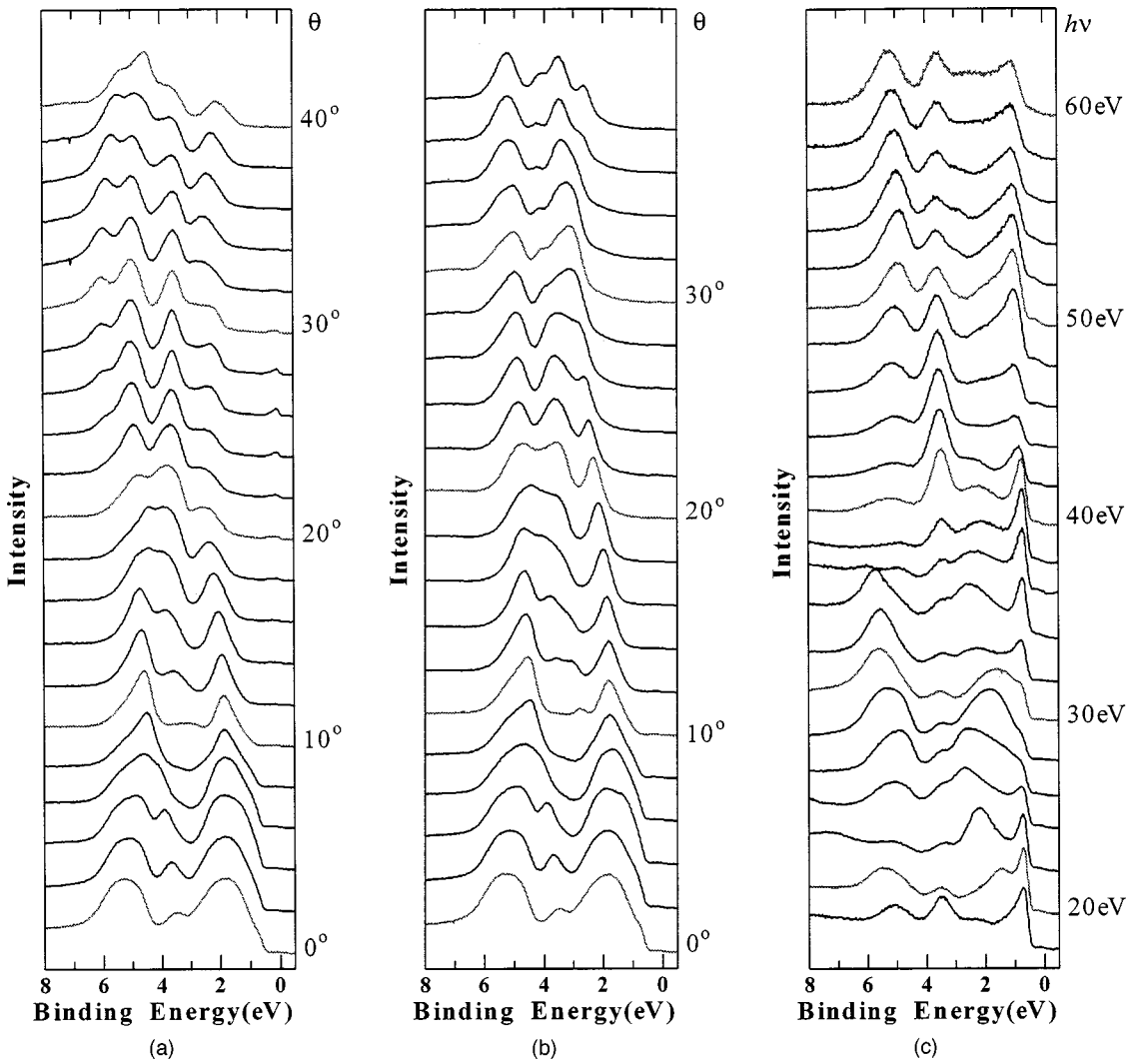

FIG. 3. ARUPS spectra of $1T$-TiS_2 along (a) $\Gamma(A)$-$M(L)$, (b) $\Gamma(A)$-$K(H)$, and (c) Γ-A (normal emission) directions.

approximation as done for the normal photoemission. A photoelectron with the kinetic energy E_K and angle θ in the vacuum should have a corresponding kinetic energy $E_K + V_0$ and a direction of the wave vector θ' in the bulk. The perpendicular component of the wave vector in the bulk is then given as

$$k_\perp = \frac{\sqrt{2m(E_K+V_0)}}{\hbar}\cos\theta'. \tag{1}$$

From the momentum conservation of the parallel component between the bulk and the vacuum, the following relation is expected:

$$k_\parallel = \frac{\sqrt{2m(E_K+V_0)}}{\hbar}\sin\theta' = \frac{\sqrt{2mE_K}}{\hbar}\sin\theta. \tag{2}$$

From this formula we get a relation between θ' and θ. Finally the perpendicular component of the wave vector is given as

$$k_\perp = \frac{\sqrt{2m}}{\hbar}\sqrt{E_K\cos^2\theta + V_0}. \tag{3}$$

Figure 2(d) shows the relation between $k_\perp$ and $k_\parallel$ in the θ-dependent ARUPS in our experiments, where the detected regions are indicated by the black area. The evaluated $k_\perp$ are in the range of 2.3–3.0 Å^{-1}. Some of the regions are rather close to the A-L or A-H line ($k_\perp = 2.76\ \text{Å}^{-1}$). The observed bands in the k-E_B diagram in Figs. 4(a), 4(b), and 4(c) are reproduced in Figs. 4(a′), (b′), and (c′) by various marks. Curves in these figures are the results of the band calculation along (a′) A-L, (b′) A-H, and (c′) Γ-A,[4] which are in qualitative agreement with the experimental results.

B. $Ni_{1/3}TiS_2$

Then we measured the ARUPS spectra of the $Ni_{1/3}TiS_2$ with changing the polar angle θ as shown in Figs. 5(a) and 5(b). The normal photoemission spectra measured with changing the photon energy $h\nu$ are shown in Figs. 5(c).

In the case of $Ni_{1/3}TiS_2$, the unit cell defined in Fig. 1 provides the extended BZ shown in Figs. 2(b) and 2(c), where the cross sections corresponding to the present experiment are indicated by the planes (1) and (2). The Γ-Z axis in $Ni_{1/3}TiS_2$ is equivalent to the Γ-A axis. The directions of the $\Gamma(A)$-$M(L)$ and $\Gamma(A)$-$K(H)$ in $1T$-TiS_2 are corresponding to the planes (1) and (2), respectively. The length of the $\Gamma(A)$-$M(L)$ equals $\Gamma(Z)$-(Δ)-$B(A)$ in plane (1). So the pe-

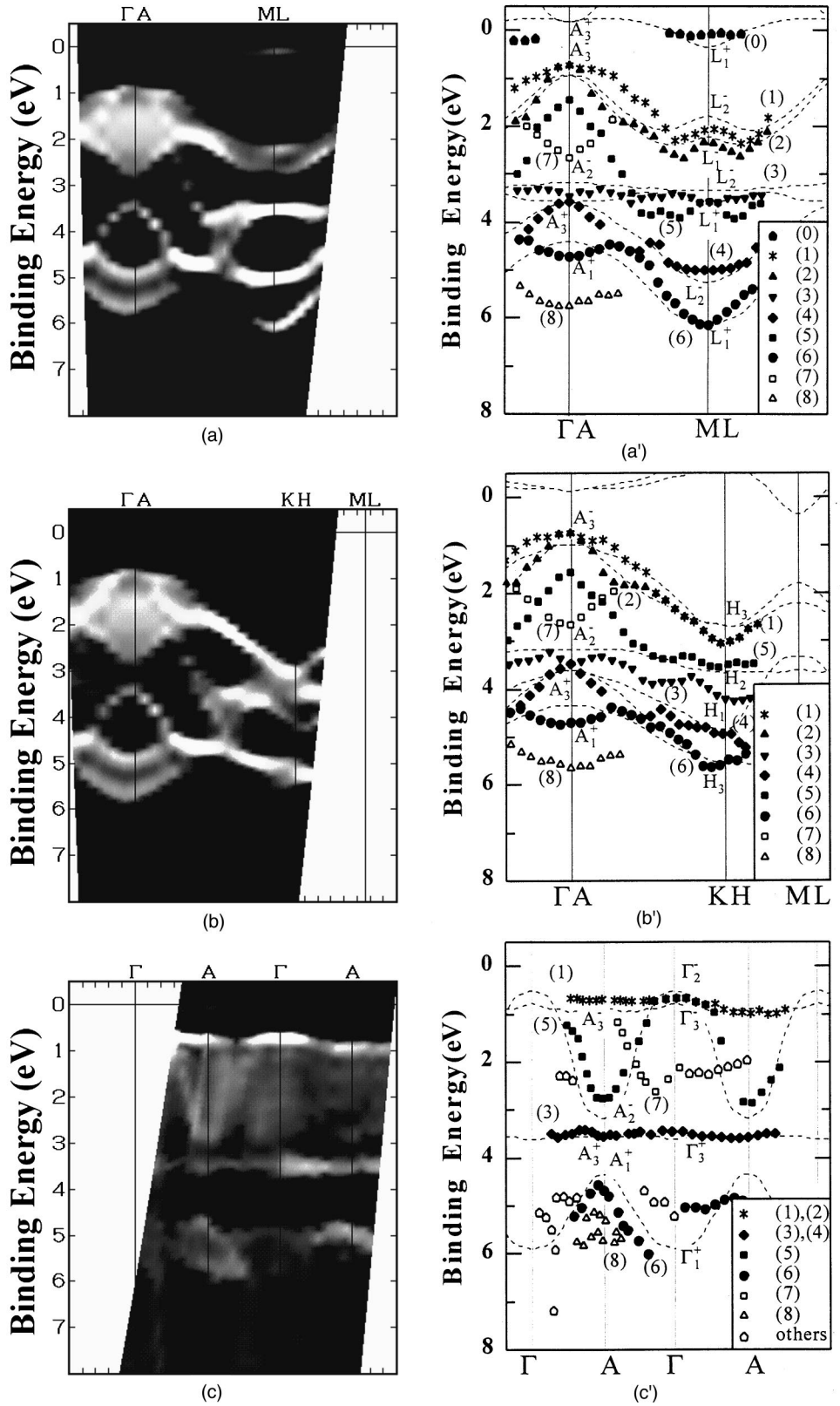

FIG. 4. The band mappings of $1T$-TiS_2 along (a) $\Gamma(A)$-$M(L)$, (b) $\Gamma(A)$-$K(H)$, and (c) Γ-A directions. The results are obtained by the deconvolution method. Comparison of the experimental results along (a′) $\Gamma(A)$-$M(L)$, (b′) $\Gamma(A)$-$K(H)$, and (c′) Γ-A directions, which are displayed with various marks, with the band calculation along (a′) A-L, (b′) A-H, and (c′) Γ-A axes.

riodicity of the band dispersions of $Ni_{1/3}TiS_2$ along the three major axes is hardly different from that of $1T$-TiS_2, because the back folding of the band structure along the $\Gamma(Z)$-(Δ)-$B(A)$ direction [Figs. 2(b)] takes place at the $B(A)$ symmetry point of the next BZ and that along the $\Gamma(Z)$-(A)-$B(A)$ direction in Fig. 2(c) takes place at the $B(A)$ point which is corresponding to the $M(L)$ points of the next BZ.

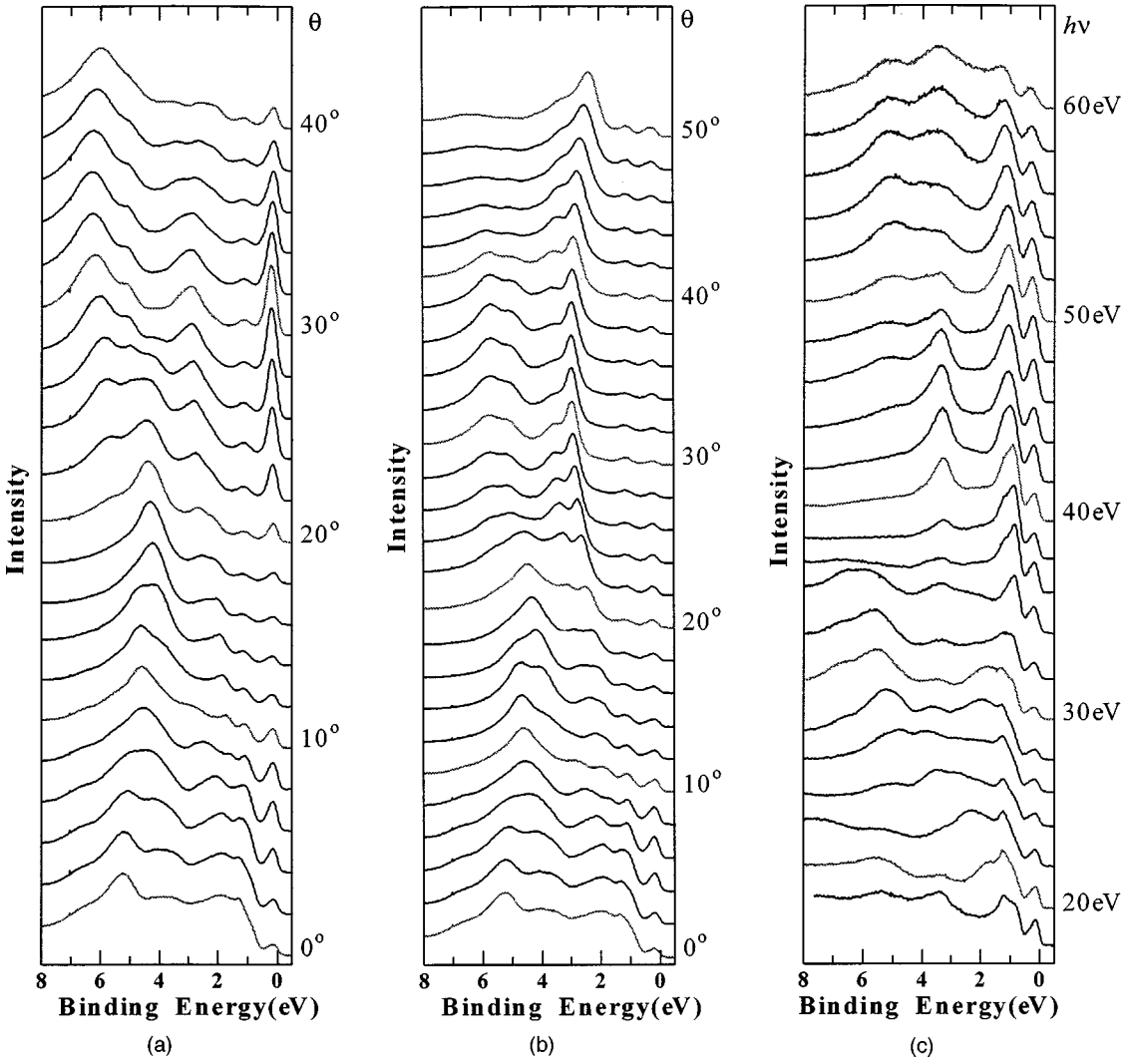

FIG. 5. ARUPS spectra of $Ni_{1/3}TiS_2$ along (a) $\Gamma(A)$-$M(L)$, (b) $\Gamma(A)$-$K(H)$, and (c) Γ-A (normal emission) directions.

For each direction of the measurement, the k-E_B diagram is drawn by the same method as applied to $1T$-TiS_2. The results shown in Figs. 6(a), 6(b), and 6(c) correspond to planes (1) and (2) as well as to the Γ-Z axis in Figs. 2(b) and 2(c). For convenience, we denote the symmetry points of BZ of $Ni_{1/3}TiS_2$ by the notation for $1T$-TiS_2.

In Figs. 6(a′) and (b′), the bands named $(A)-(M)$ are revealed. We first notice that some structures show similar but strongly modified behavior between $1T$-TiS_2 and $Ni_{1/3}TiS_2$. [For example, structure (1) vs structure (B)]. On the other hand, some new structures, for example, the (K) and (L) bands appear in $Ni_{1/3}TiS_2$. The (K) band appears just below E_F in wide wave vector regions and hardly shows dispersion. Its intensity is enhanced around $\theta=26°$ (ML) in Fig. 5(a) and around $\theta=6°$ in both Figs. 5(a) and 5(b). We stress this enhancement by using (A). The (L) band appears at the binding energy (E_B) of $\sim$1 eV and hardly shows dispersion for both axes in Figs. 6(a′) and (b′) except for the region near the $\Gamma(A)$ point. For the evaluation of dispersion along the Γ-$Z(\Gamma$-$A)$ axis, the same inner potential $V_0=11$ eV as for $1T$-TiS_2 is employed. In Fig. 6(c′) the bands $(B)-(L)$ are clarified. Though we tried to compare our results with the APW band calculation of $Ni_{1/3}TiS_2$,[10] we could not get any meaningful information, because there are too many bands in the calculation. So we try to directly compare the experimental results of $Ni_{1/3}TiS_2$ with those of $1IT$-TiS_2.

IV. DISCUSSION

Before discussing the electronic states of $Ni_{1/3}TiS_2$, we first review the electronic structure of $1T$-TiS_2. It is thought in $1T$-TiS_2 that the S atom is nearly S^{2-} and the Ti atom is nearly Ti^{4+} with the $3d^0$ configuration. According to the simple crystal-field theory, the Ti $3d$ states of $1T$-TiS_2 are split into the ''t_{2g}'' and ''e_g'' states. The S $3p$ states are strongly hybridized with the Ti $3d$''e_g'' states and make the bonding and antibonding states with the bonding bands filled with electrons. The ''t_{2g}'' states are the nonbonding bands and a small band gap exists between the nonbonding and bonding states.

Comparing the observed bands with the results of band calculation, we can identify some of these bands. The observed bands (1), (2), (3), and (4) in Fig. 4 might be corresponding to A_3^--L_2^--H_3 (1), A_3^--L_1^--H_3 (2), A_3^+-L_1^+-H_1 (3), A_3^+-L_2^--H_3 (4), respectively. These bands do not have appreciable dispersions along the Γ-A axis as shown in Fig. 4(c). On the other hand, both the (5) and (6) band have remarkable dispersions along the Γ-A

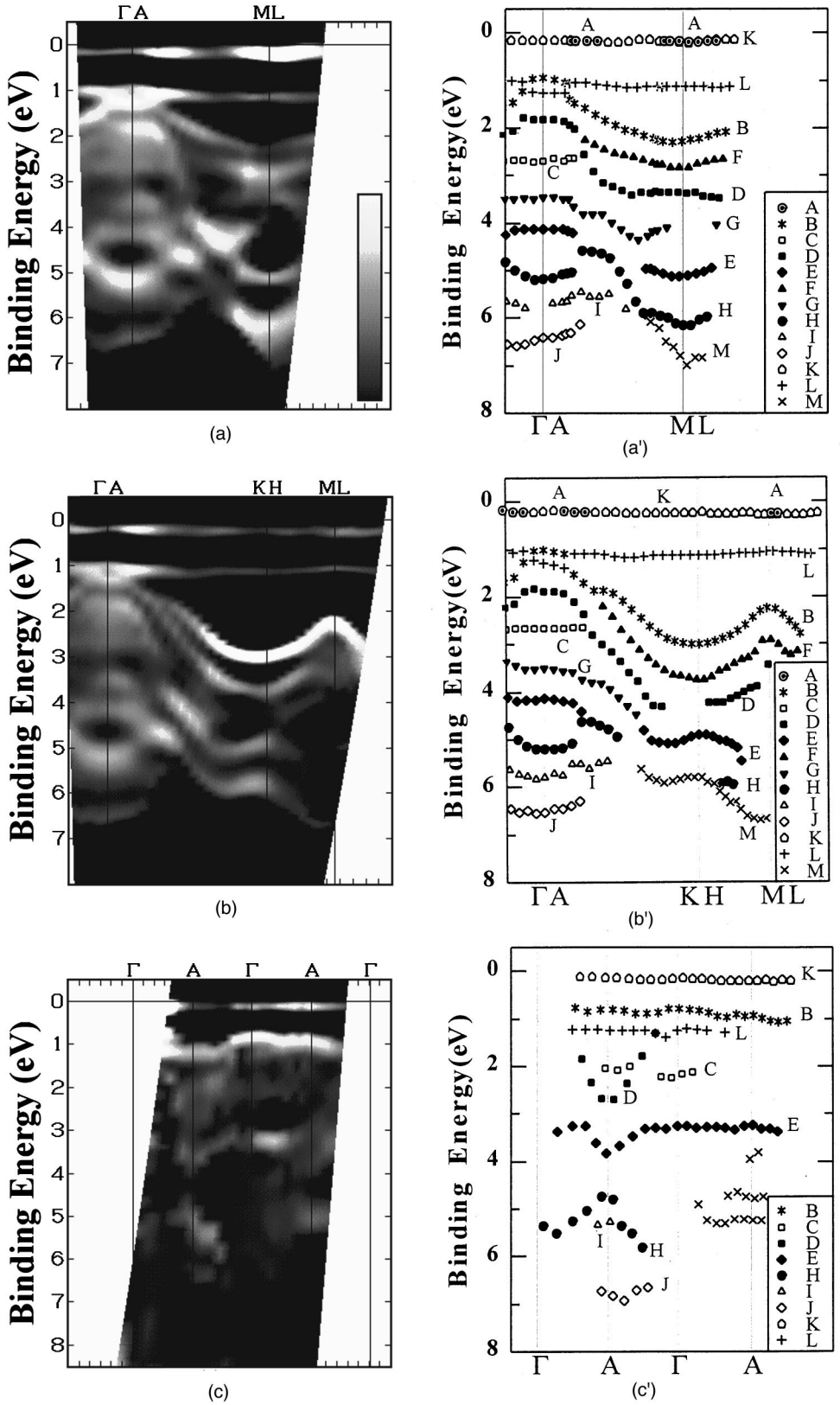

FIG. 6. The band mappings of $Ni_{1/3}TiS_2$ along (a) $\Gamma(A)$-$M(L)$, (b) $\Gamma(A)$-$K(H)$, and (c) Γ-A directions, by means of the deconvolution method. The dispersions along (a′) $\Gamma(A)$-$M(L)$, (b′) $\Gamma(A)$-$K(H)$, and (c′) Γ-A directions, are displayed with the conventional method with using different marks.

axis. In the previous section, we have evaluated the $k_\perp$ component of the θ-dependent ARUPS spectra. The $k_\perp$ value of the photoemission structures plotted in Figs. 4(a) and 4(b) are not exactly along the A-L and A-H directions. We assign the bands (5) and (6) to the states represented by the A_2^--L_2^--H_2 and A_1^+-L_1^+-H_3 states. We see a great discrep-

ancy between the dispersions (5) and A_2^--L_2^--H_2 near the $\Gamma(A)$ point in Fig. 4(a′). The corresponding experimental points near the Γ-A axis are far away from the A point [Fig. 2(d)]. Therefore a strong dispersion [Fig. 4(c′)] provides much smaller E_B for the experimental points. The discrepancy from A_2^--L_2^--H_2 dispersion is thus consistently interpreted. Although both (7) and (8) bands have remarkable dispersions along the horizontal axes around the $\Gamma(A)$ symmetry point, they seem to have no direct counterparts in the band calculation shown in Figs. 4(a′) and 4(b′).

Now we discuss the results of the intercalated $Ni_{1/3}TiS_2$. Before discussing the dispersion of the electronic states, the surface condition is considered. The cleavage is thought to take place in the van der Waals gap where the Ni atoms are intercalated. One half of the Ni atoms stays on the sample surface to be measured and the other half of the Ni atoms goes away from the sample surface. Although the $\sqrt{3}\times\sqrt{3}$ super structure was clarified by LEED on the cleaved surface, such a structure was not confirmed by STM. This result shows that the Ni atoms are ordered in the bulk but disordered just on the surface. The random (or statistical) distribution of Ni atoms just on the surface (or surface disorder) may induce some effect on the surface-related electronic states. Since the ultraviolet photoemission is a rather surface sensitive probe, one must pay some attention to the surface disorder effect.

The origins of the (K) and (L) bands will be discussed later. Most of the bands except for the bands (K) and (L) have counterparts in $1T$-TiS_2, although the dispersions are appreciably modified by intercalation. The imhomogeneous energy shifts and splittings of various bands suggest the break down of the rigid-band shift model. Judging from the clear dispersing behaviors, the (D) and (H) bands in $Ni_{1/3}TiS_2$ are thought to be corresponding to the (5) and (6) band in $1T$-TiS_2, which have the S $3p\pi$ character and remarkable dispersions with both $k_\parallel$ and $k_\perp$. We notice, however, some differences in the Ni intercalation compound compared with $1T$-TiS_2. For example, the top of the band (D) is slightly depressed (flat) and the band width along the $\Gamma(A)$-$M(L)$ direction is appreciably reduced in $Ni_{1/3}TiS_2$. The E_B of the band (H) near the Γ point is much larger than the corresponding E_B of the band (6) in $1T$-TiS_2. In addition, we notice an appearance of a new branch (M) near the ML point in Fig. 6(a′) and in the region of the KH (ML) points in Figs. 6(b′). These bands are thought to be strongly influenced by the hybridization effects with the Ni $3d$ states in regard to the energy positions of the bands, dispersions, and band broadening. It is noticed that the bands D and H in $Ni_{1/3}TiS_2$ are slightly diffuse or broader than the bands (5) and (6) in $1T$-TiS_2. The possibility that the abovementioned surface disorder may provide additional broadening to the spectra cannot be discarded.

The bands (B) and (E) in $Ni_{1/3}TiS_2$ are corresponding to the bands (1) [or (2)] and (4) in $1T$-TiS_2, respectively, and the dispersion behaviors are qualitatively similar between $Ni_{1/3}TiS_2$ and $1T$-TiS_2. Both of these bands might not be strongly hybridized with the Ni $3d$ states, because the modification by intercalation is not large. It is also noticed that the broadening of the bands B and E is not much different from that of (1) and (4). This is understood by considering that the hybridization with the Ni $3d$ states is weak in the bands B and E. Then the surface disorder of Ni atoms may not much influence their broadening.

Meanwhile, the bands (G) and (F) are thought to be corresponding to the bands (3) and (2) [or (1)] from their energy positions, although they are remarkably modified by the Ni interaction. For example, the (G) band is now clearly separated from the (E) band near the $\Gamma(A)$ point, in contrast to the unresolved separation between the bands (3) and (4) in $1T$-TiS_2. Furthermore, the (G) band has larger dispersions along the horizontal axes than the (3) band in $1T$-TiS_2. The (F) band is also separated from the (B) band even near the $\Gamma(A)$ point in contrast to the bands (2) and (1) in $1T$-TiS_2. Both (G) and (F) bands are understood to be appreciably modified by the hybridization with the Ni $3d$‘‘e_g’’ states. The broadening of the bands G and F is more than that of the bands (3) and (2), resulting from the hybridization, whereas the additional contribution from the surface disorder cannot be discarded here again.

Summarizing these discussions, the S $3p\pi$ bands [bands (5) and (6) in $1T$-TiS_2] are appreciably hybridized with the Ni $3d$‘‘e_g’’ states providing the dispersions of the bands (D) and (H). Even an appearance of the new branch (M) may be attributed to this hybridization. The half of S $3p\sigma$ bands [(B) and (E)] is hardly influenced by the Ni intercalation, whereas the another half of S $3p\sigma$ bands [(G) and (F)] is thought to be well hybridized with the Ni $3d$‘‘e_g’’ states. This might be related to the symmetries of the bands in $Ni_{1/3}TiS_2$, where the Ni atom occupies the octahedral site and the Ni $3d$‘‘e_g’’ states face to the S atoms making covalent bonds with the S $3p$ state.

If the dispersions of $Ni_{1/3}TiS_2$ (Figs. 6) and $1T$-TiS_2 (Figs. 4) are compared, it is clear that the bands (C) and (I) correspond to the bands (7) and (8) in $1T$-TiS_2. From the absence of corresponding band in the band calculation of $1T$-TiS_2, the bands (7) and (8) in $1T$-TiS_2 are thought to be surface states. The guest Ni atoms influence the surface state in $Ni_{1/3}TiS_2$. The low concentration of Ni atoms randomly distributed on the surface, however, reduces the dispersion of the surface states. The origins of these surface states are not yet clear and require future investigation.

Now we discuss the origin of the bands (K) and (L) which appear newly in $Ni_{1/3}TiS_2$. Both the (K) band located at $E_B = 0.2$ eV and the (L) band at $E_B = 1 \sim 1.2$ eV show negligible dispersion. One may first think of a possibility that they may be related to the $3d$ states of the surface disordered Ni atoms. The Ti $2p$ and Ni $2p$ core resonance photoemission, however, denies such a possibility as explained later. The intensity of the (K) band is very strong around the $M(L)$ point when scanned along the $\Gamma(A)$-$M(L)$ axis compared with the (O) band in $1T$-TiS_2. At first, we examine the possibility that this state at $E_B = 0.2$ eV is made by the charge transfer from the Ni to the Ti.[12] If the electron of the Ni is partially transferred to the empty Ti $3d$‘‘t_{2g}’’ state without modification of the band structure, the band observed near the $M(L)$ point in $1T$-TiS_2 should move downward. Then the dispersion of the ‘‘t_{2g}’’ state will be observed in wider energy range below E_F in $Ni_{1/3}TiS_2$. However, this band (K) shows rather flat dispersions in wide wave vector regions. So such a simple interpretation of this structure as the filled Ti‘‘t_{2g}’’

band will not be satisfactory. In order to know the detailed origin of the (*K*) band, we have measured the Ti $2p$-core absorption related resonance photoemission.[15] The results have suggested that the state at $E_B=0.2$ eV shows the Ti ''e_g'' character rather than the Ti ''t_{2g}'' or the Ni $3d$ character in contrast to our supposition. This discrepancy can be solved by considering a system with the Ti $3d^1$ ground state in $Ni_{1/3}TiS_2$ which is made by the charge transfer (CT) from the Ni to Ti atom. Okada *et al.* discussed the character of the sharp photoemission structure often found in Ti^{3+} compounds just below E_F by considering the $d^2\underline{L}$ and d^1 configurations in the ground state.[16,17] They interpreted such a structure as the split-off state or the bonding state between the $d^1\underline{L}$ and d^0 final states. In the present case, the ground state of $Ni_{1/3}TiS_2$ can be represented by a linear combination of the $d^1(t_{2g})$ and $d^2(t_{2g},e_g)\underline{L}$ states. Then the photoemission final state is given by a linear combination of the d^0, $d^1(t_{2g})\underline{L}$, and $d^1(e_g)\underline{L}$ states. The observed resonance enhancement of this structure for the Ti $2p\rightarrow e_g$ excitation is attributed to the $d^1(t_{2g})\underline{L}$ final state with emitting the e_g electron in the direct recombination process. The p-d charge transfer energy Δ can be defined as $E(d^2\underline{L})-E(d^1)$ for the $3d^1$ system. In the valence band photoemission final state of this system, the energy difference between the $d^1\underline{L}$ and d^0 final states is given by Δ-U_{dd}, where U_{dd} represents the $3d$ electron correlation energy. These states hybridize via an off-diagonal matrix element $V_{\rm eff}$ making a large splitting between the bonding and antibonding states. The energy difference between these two states is estimated to be about 7 eV. In the experimental results in Figs. 6, one notices a very weak shoulder structure (*J*) at $E_B\sim 6.5$ eV, which only appears with intercalation. It is possible that this (*J*) band is the counterpart of the (*K*) band in this model, although another possibility that the counterpart is hidden below the strong photoemission structures in the region from $E_B=4-6$ eV cannot be discarded.

The (*L*) band located at $E_B=1\sim 1.2$ eV shows a negligible dispersion of less than 0.2 eV along the horizontal and vertical axes. This feature suggests that this band is due to a localized state rather than a bandlike state. From the resonance photoemission results for the Ti and Ni $3p$- and $2p$-core excitations, this state is found to have both the Ni $3d$ and Ti $3d$ characters. It is remembered that the Ni $3d$ states are split into the ''t_{2g}'' and ''e_g'' states. The wave functions of the ''t_{2g}'' state consist of three base functions. The ''t_{2g}'' states hardly make the bonding states with the S atoms, because their wave functions are not directed to the S atoms. The component of the Ni d_{z^2} state (here the *z* refers to the crystallographic axis perpendicular to the TiS_2 layer) made of these ''t_{2g}'' states, however, faces toward the upper and the lower Ti atoms making the bonding and antibonding states. These states are not band states but have a localized character, because the distance between the equivalent bonding (antibonding) states along the *z* axis is very large in the crystal as shown in Fig. 1.

We have now arrived at a conclusion that the band (*L*) mainly originates from the bonding state between the Ni $3d_{z^2}$ and Ti $3d_{z^2}$ states. Namatame *et al.* already performed the angle resolved inverse photoemission spectroscopy (ARIPES) on $Ni_{1/3}TiS_2$ (Ref. 14) and found the antibonding state between the Ni $3d_{z^2}$ and Ti $3d_{z^2}$ states around 2 eV above E_F with a rather small dispersion. The energy splitting between the bonding and antibonding states is estimated as about 3 eV. This interpretation is supported by the ARUPS experiments on $Co_{1/3}TiS_2$, $Fe_{1/3}TiS_2$, and $Mn_{1/4}TiS_2$ which will be reported elsewhere.

V. CONCLUSION

Strong modification of the valence band structures and band dispersions in an intercalation compound $Ni_{1/3}TiS_2$ are revealed by the conventional angle resolved photoemission spectroscopy. The hybridization of the S derived states with the Ni ''e_g'' states is thought to be predominantly modifying the band dispersions parallel to the layer plane. The new band at $E_B=1.0$ eV is attributed to the bonding band between the Ti $3d_{z^2}$ and Ni $3d_{z^2}$ states. On the other hand, the band at $E_B=0.2$ eV is interpreted as a spit-off state or the bonding state between the d^0 and $d^1\underline{L}$ final states which arise from the $d^1(t_{2g})$ and $d^2(t_{2g},e_g)\underline{L}$ initial states. The counter part of this state (antibonding state between the d^0 and $d^1\underline{L}$ final states) might be observed in the region of $E_B=6.0$ eV.

ACKNOWLEDGMENTS

The authors acknowledge H. Shigeoka, Professor A. Kakizaki, and Professor H. Daimon for partial support and useful advice. This work was performed under the approval of the Photon Factory Advisory Committee. This work was partially supported by a Grant-in-Aid for COE research (Grant No. 10 CE 2004) of the Ministry of Education, Science, Sports and Culture, Japan.

*Present address: Japan Synchrotron Radiation Research Institute (JASRI), 323-3 Mihara, Mikazuki-cho, Sayo-gun, Hyogo 679-5198, Japan.

†Author to whom correspondence should be addressed.

‡Present address: Department of Materials Sciences, Hiroshima University, Higashi Hiroshima 739-8526, Japan.

[1] C. H. Chen, W. Fabian, F. C. Brown, K. C. Woo, B. Davies, and B. DeLong, Phys. Rev. B **21**, 615 (1980).

[2] J. J. Barry, H. P. Hughes, P. C. Klipstein, and R. H. Friend, J. Phys. C **16**, 393 (1983).

[3] S. Nohara, H. Namatame, H. Matubara, M. Fujisawa, M. Naitou, S. Tanaka, H. Negishi, M. Inoue, H. Sakamoto, A. Misu, and S. Suga, J. Phys. Soc. Jpn. **60**, 3882 (1991).

[4] A. Zunger and A. J. Freeman, Phys. Rev. B **16**, 906 (1977).

[5] M. Inoue, Y. Muneta, H. Negishi, and M. Sasaki, J. Low Temp. Phys. **63**, 235 (1986).

[6] M. Inoue, Y. Muneta, H. Negishi, and M. Sasaki, J. Magn. Magn. Mater. **53**, 131 (1985).

[7] H. Negishi, A. Shoube, H. Takahashi, Y. Ueda, M. Sasaki, and M. Inoue, J. Magn. Magn. Mater. **67**, 179 (1987); M. Inoue, M. Matsumoto, H. Negishi, and H. Sakaki, *ibid.* **53**, 131 (1985).

[8] M. Koyano, H. Negishi, Y. Ueda, M. Sasaki, and M. Inoue, Solid State Commun. **62**, 261 (1987).

[9] T. Yamasaki, N. Suzuki, and K. Motizuki, J. Phys. C **20**, 395 (1987).

[10] N. Suzuki, T. Yamazaki, and K. Mochizuki, J. Phys. Soc. Jpn. **58**, 3280 (1989).
[11] Y. Ueda, H. Negishi, M. Koyano, M. Inoue, K. Soda, H. Sakamoto, and S. Suga, Solid State Commun. **57**, 839 (1986).
[12] Y. Ueda, K. Fukushima, H. Negishi, M. Inoue, M. Taniguchi, and S. Suga, J. Phys. Soc. Jpn. **56**, 2471 (1987).
[13] A. Fujimori, S. Suga, H. Negishi, and M. Inoue, Phys. Rev. B **38**, 3676 (1988).
[14] H. Namatame, S. Nohara, H. Negishi, M. Inoue, and S. Suga, Surf. Sci. **242**, 294 (1991).
[15] A. Kimura, S. Suga, and T. Matsushita (unpublished).
[16] K. Okada and A. Kotani, J. Electron Spectrosc. Relat. Phenom. **62**, 131 (1993).
[17] K. E. Smith and V. E. Henrich, Phys. Rev. B **38**, 5965 (1988).